Published in final edited form as:

Nat Struct Mol Biol. 2017 March ; 24(3): 309–315. doi:10.1038/nsmb.3375.

Mechanism and Timing of Mcm2–7 Ring Closure During DNA Replication Origin Licensing

Simina Ticau[1,†], **Larry J. Friedman**[2], **Kanokwan Champasa**[1], **Ivan R. Corrêa Jr**[3], **Jeff Gelles**[2,*], and **Stephen P. Bell**[1,*]

[1]Howard Hughes Medical Institute, Department of Biology, Massachusetts Institute of Technology, Cambridge, MA 02139 USA

[2]Department of Biochemistry, Brandeis University, Waltham, MA 02454, USA

[3]New England Biolabs, Ipswich, MA 01938 USA

Abstract

Opening and closing of two ring-shaped Mcm2–7 DNA helicases is necessary to license eukaryotic origins of replication although the mechanisms controlling these events are unclear. The origin-recognition complex (ORC), Cdc6 and Cdt1 facilitate this process, establishing a topological link between each Mcm2–7 and origin DNA. Using colocalization single-molecule spectroscopy and single-molecule FRET (Förster resonance energy transfer), we monitored *S. cerevisiae* Mcm2–7 ring opening and closing during origin licensing. The two Mcm2–7 rings are open during initial DNA association and close sequentially, concomitant with release of their associated Cdt1. ATP hydrolysis by Mcm2–7 is coupled to ring closure and Cdt1 release, and failure to load the first Mcm2–7 prevents recruitment of the second Mcm2–7. Our findings identify key mechanisms controlling the Mcm2–7 DNA-entry gate during origin licensing and reveal that the two Mcm2–7 complexes are loaded by a coordinated series of events with implications for bidirectional replication initiation and quality control.

[*]Co-corresponding authors: Stephen P. Bell, spbell@mit.edu, phone: 617-253-2054, Jeff Gelles, gelles@brandeis.edu, phone: 781-736-2377.

[†]Current address: VL34 Inc., Cambridge, MA 02139

Code availability

Links to code are included in the methods, Supplementary Figure 3 legend and Supplementary Table 1 description.

Data availability

The data that support the findings of this study are available from the corresponding authors upon reasonable request.

Author contributions

S.T. performed all experiments with feedback from J.G., L.J.F. and S.P.B. except ensemble FRET studies which were performed by K.C. I.R.C. prepared essential reagents. S.T., L.J.F. and J.G. analyzed the data. S.P.B. composed the paper with input from all authors. S.P.B. and J.G. directed the project.

Competing Financial Interests Statement

The authors declare no competing financial interests.

Introduction

During eukaryotic DNA replication, origins of replication are licensed when two copies of the ring-shaped, heterohexameric Mcm2–7 helicase topologically encircle origin DNA[1]. This linkage is established when the interface between Mcm2 and Mcm5 (Mcm2-Mcm5 gate) is opened to allow DNA to enter the central channel of the helicase and then closed to prevent DNA release[2,3]. The two Mcm2–7 complexes are loaded sequentially. One Mcm2–7, in complex with Cdt1, is initially recruited to origin DNA bound by the origin-recognition complex (ORC) and Cdc6[4–6]. This intermediate rapidly releases Cdc6 and then Cdt1[6–8]. A second Cdc6 and Cdt1-Mcm2–7 subsequently associate with ORC and the first Mcm2–7[8,9], followed by release of Cdc6, Cdt1 and ORC[8]. The net result is a head-to-head Mcm2–7 double hexamer that encircles the origin DNA and is poised for bidirectional initiation[4,10].

ATP binding and hydrolysis is critical for helicase loading. ATP binding is required for the initial DNA association of the three helicase-loading proteins and Mcm2–7[11,12]. ATP hydrolysis is required to move beyond this initial association and complete Mcm2–7 loading[6,13,14]. ORC, Cdc6 and Mcm2–7 all bind and hydrolyze ATP. Although not required for helicase loading, ORC ATP hydrolysis is required for the repetition of this event[15]. Cdc6 ATP hydrolysis is also not required for helicase loading[13,14,16], however, it is required for a quality control mechanism that releases incompletely loaded Mcm2–7 from DNA[13,14,17]. Mcm2–7 ATP hydrolysis by at least a subset of the six Mcm2–7 ATPase motifs is required for helicase loading[13,14], however, it remains unclear which event(s) depends on the action of these ATPases.

Although previous studies have revealed both the order of protein associations during helicase loading and their regulation[18], the timing and mechanism of the key event of Mcm2–7 ring opening and closing remains unclear. ATP binding at the Mcm2-Mcm5 interface is proposed to close the Mcm2–7 ring[3] and this is supported by EM studies of ATPγS-bound Mcm2–7[9]. In contrast, in the presence of ATP structural studies show Mcm2–7 in an open state[19,20]. The status of the Mcm2-Mcm5 gate in the initially recruited Cdt1-Mcm2–7 complex is unknown. The sequence and structural similarity of ORC–Cdc6 to sliding clamp loaders has led to a hypothesis that binding to ORC and Cdc6 opens the Mcm2–7 ring[7] but this remains to be tested.

Using a single-molecule FRET-based approach, we have examined the timing and mechanism of Mcm2–7 ring opening and closing and its relationship to other events of origin licensing. We find that Mcm2–7 is in an open state upon initial binding and that this state is independent of Cdt1 binding. Mcm2–7 ring closure occurs independently for each Mcm2–7 at a time that is concomitant with Cdt1 release. Interestingly, we find that ATP hydrolysis by Mcm5-Mcm3 is required for ring closure and Cdt1 release. Preventing these events inhibits recruitment of the second Mcm2–7 ring. Our findings provide important insights into the mechanism of helicase loading and reveal attributes of this event that favor double-hexamer formation and quality control.

An assay for Mcm2-Mcm5 gate status

Based on the closed Mcm2–7 ring structure[21], we attached donor (D) and acceptor (A) fluorophores to Mcm2 and Mcm5 at positions where FRET should increase in the closed state (Figs. 1A and S1A). This fluorescent variant (Mcm2–7^{25FRET}) functioned at near wild-type levels in bulk helicase-loading assays performed with purified proteins (Supplementary Fig. 1B–D). To measure Mcm2–7 DNA association and changes in apparent FRET efficiency (E_{FRET}) during helicase loading, we incubated surface-attached fluorescent origin DNA with purified Mcm2–7^{25FRET}, ORC, Cdc6, and Cdt1[8]. Co-localization of the protein- and DNA-associated fluorophores was indicative of DNA binding. Alternating excitation of acceptor (Fig. 1B, Supplementary Figs. 2 and 3A, panel i) and donor (Figs. 1B and Supplementary Figs. 2 and 3A, panels ii-iv) allowed us to monitor Mcm2–7 binding to individual DNAs and calculate E_{FRET} for bound Mcm2–7^{25FRET}. Long-lived sequential increases in Mcm2–7-associated fluorescence revealed the first and second Mcm2–7 binding events (Fig. 1B and Supplementary Fig. 3A[8]). We focused on events in which simultaneous increases in both acceptor-excited and total donor-excited fluorescence (e.g., Fig. 1B i and iii, black arrows) indicated that an Mcm2–7^{25FRET} with both D and A fluorophores was binding. After initial binding, Mcm2–7^{25FRET} showed relatively high D emission and weak A emission (e.g. Fig. 1Bii, ~850 s), producing a low E_{FRET} value. Long-lived Mcm2–7^{25FRET} molecules subsequently displayed decreased D emission and increased A emission, indicative of increased E_{FRET} (e.g., Fig. 1B ii, ~880 s).

Analysis of a large number of Mcm2–7^{25FRET} helicase-loading trajectories revealed evidence for two major types of DNA-Mcm2–7 complexes with distinct E_{FRET} values (Fig. 1C). Early after DNA binding (<15 s), Mcm2–7^{25FRET} was predominantly in an E_{FRET} state of ~0.18, (Fig. 1C, Supplementary Fig. 3B and Supplementary Table 1). At intermediate times (15–75 s), we observed a mixture of E_{FRET} ~0.18 and E_{FRET} ~0.36 states. At longer times (>75 s), we saw almost entirely E_{FRET} ~0.36. A similar set of distributions was observed for binding of a second Mcm2–7^{25FRET}, except that an intermediate E_{FRET} ~0.28 value was seen at early time points (Supplementary Fig. 3C and Supplementary Table 2). This intermediate value suggests that the first Mcm2–7 remains in the E_{FRET} ~0.36 state while the second Mcm2–7 is initially in the E_{FRET} ~0.18 state. These distributions are consistent with a transition by both the first and second Mcm2–7 complexes from an open Mcm2-Mcm5 gate (E_{FRET} ~0.18) to a closed Mcm2-Mcm5 gate (E_{FRET} ~0.36). A similar transition between discrete low and high E_{FRET} states during helicase loading was observed for an alternative Mcm2–7 construct in which Mcm2 was fluorescently labeled at a different location (Supplementary Fig. 3D), consistent with the idea that E_{FRET} increase is caused by a conformational change that reduces the distance between Mcm2 and Mcm5.

In support of the higher E_{FRET} state representing a closed Mcm2-Mcm5 gate, Mcm2–7^{25FRET} DNA complexes with time-averaged E_{FRET} values greater than 0.25 correlated with long-lived (>100 s) DNA associations (Fig. 1D). Consistent with higher E_{FRET} being caused by changes within an individual Mcm2–7, elevated E_{FRET} was seen only when D and A were on the same Mcm2–7 hexamer (Supplementary Fig. 2A). Furthermore, once molecules reached the E_{FRET} ~0.36 state, no persistent excursions at or below E_{FRET} = 0.18 were observed (>5 s; N=0/57), consistent with a stably closed Mcm2–7 ring[4]. These findings

combined with subsequent observations lead us to conclude that the E_{FRET} ~0.18 and ~0.36 states of individual Mcm2–7^{25FRET} complexes represent the open and closed conformation of the Mcm2-Mcm5 gate, respectively.

Cdt1 release is concomitant with Mcm2–7 ring closure

Because Cdc6 and Cdt1 sequentially dissociate from the DNA after facilitating initial Mcm2–7 binding[8], we asked if either of these events correlated with Mcm2-Mcm5 gate closure. For the first Mcm2–7 association, we compared the times of gate closure, as assessed by attainment of the E_{FRET} ~0.36 state, with previously determined distributions of first Cdc6 and Cdt1 release times (Fig. 2A and reference[8]). In each case, these times were measured relative to initial Mcm2–7 DNA association. The average time for Cdc6 release was much shorter than the average gate-closure time. In contrast, the distributions of times for Cdt1 release and gate-closure were similar, supporting a connection between these events. Because Cdt1 release is slower for the second Mcm2–7 than the first[8], we asked if Mcm2-Mcm5 gate closure for the second Mcm2–7 was similarly delayed. Indeed, the times of gate closure after arrival of the second Mcm2–7 showed a similar distribution to the times of the second Cdt1 release (Fig. 2B). Thus, for both the first and second Mcm2–7, ring closure was concomitant with Cdt1 release.

For the comparisons between the previously determined Cdt1 release times and Mcm2–7^{25FRET} ring closure times to be valid, the kinetics of the Mcm2–7^{25FRET} loading reaction should be similar to that of the singly-modified Mcm2–7 (Mcm2–7^{4SNAP}, Mcm2–7 with SNAP at the N-terminus of Mcm4) used in the previous determination of Cdt1 release times[8]. To test for this, we made Mcm2–7^{25FRET}*, a preparation in which only Mcm5-SNAP is attached to a fluorophore but Mcm2-CLIP is still present in the complex. Whit only a single fluorophore on Mcm2–7^{25FRET}*, we could simultaneously measure the DNA association and dissociation of Mcm2–7^{25FRET}* and a second protein labeled with a second fluorophore. Although helicase loading was inhibited when Mcm2–7^{25FRET}* was combined with labeled Cdt1, labeled ORC and Cdc6 were compatible with Mcm2–7^{25FRET}*. Importantly, we observed similar release times of Cdc6 and ORC whether we used Mcm2–7^{25FRET}* or Mcm2–7^{4SNAP} (Supplementary Fig. 4A–C). Although we could not measure the kinetics of Cdt1 in the presence of Mcm2–7^{25FRET}, we note that the times of Cdc6 and ORC release encompass the times of Cdt1 release. Thus, the kinetics of the helicase loading reaction is not dramatically changed by the SNAP and CLIP proteins inserted into Mcm5 and Mcm2 present in Mcm2–7^{25FRET}.

The similar kinetics of Cdt1 release and Mcm2–7 ring closure suggested that Cdt1 binding to Mcm2–7 holds the Mcm2-Mcm5 gate open. To address this possibility, we monitored E_{FRET} for Mcm2–7^{25FRET} in the absence of DNA, ORC and Cdc6. Whether Mcm2–7^{25FRET} was directly tethered to the slide in the absence of Cdt1 or tethered to the slide indirectly via Cdt1, the Mcm2-Mcm5 gate was predominantly in an open (E_{FRET} ~0.16) state with smaller populations in higher E_{FRET} states (Fig. 2C and Supplementary Table 3). Interestingly, the higher E_{FRET} populations were reduced for Cdt1-bound Mcm2–7 (Supplementary Table 3), suggesting Cdt1 increases the already high bias of Mcm2–7 toward an open (E_{FRET} ~0.16) state. Consistent with Cdt1-Mcm2–7 being in an largely open state in contrast to the closed

state of loaded Mcm2–7, we measured solution E_{FRET} values for free Cdt1–Mcm2–7^{25FRET} and loaded Mcm2–7^{25FRET}. Although the absolute values are different from those seen in the single-molecule experiments due to incomplete protein labeling (only doubly-labeled proteins were assessed in the single-molecule setting), we observed higher solution E_{FRET} values for loaded Mcm2–7^{25FRET} (0.129 ± 0.004) than for free Cdt1–Mcm2–7^{25FRET} (0.076 ± 0.002). These findings are consistent with previous low-resolution structural studies showing that free Mcm2–7 has an open Mcm2-Mcm5 gate[19,20]. We conclude that Cdt1 is not required to prevent Mcm2–7 ring closure, but Cdt1-bound Mcm2–7 may more strongly favor the open state.

ORC release occurs after closure of both Mcm2–7 rings

To simultaneously monitor in three-color experiments the status of the Mcm2-Mcm5 gate and release of fluorescently-labeled proteins in three-color experiments from individual DNAs, we labeled Mcm2 and Mcm5 with a fluorophore and a quencher, respectively (Mcm2–$7^{25quench}$, Fig. 3A). Bulk assays showed that Mcm2–$7^{25quench}$ retains ~50% of wild-type helicase-loading activity (Supplementary Fig. 1C and 1D). Consistent with our Mcm2–7^{25FRET} studies, this complex showed high fluorescence upon initial DNA binding (gate open) and reduced fluorescence thereafter (gate closed, Fig. 3B and Supplementary Fig. 4D). Experiments combining Mcm2–$7^{25quench}$ with differentially labeled Mcm2–7 (Mcm2–7^{JF646}), showed that the Mcm2-Mcm5 gate of the first Mcm2–7 did not reopen once closed, including during loading of the second Mcm2–7 (Fig. 3C).

As with Mcm2–7^{25FRET}, labeled Cdc6 and ORC were compatible with Mcm2–$7^{25quench}$ but fluorescently-labeled Cdt1 inhibited helicase loading when combined with this form of Mcm2–7. Consistent with Cdc6 being released before Cdt1[8], labeled Cdc6 was always released prior to Mcm2–$7^{25quench}$ gate closure (Fig. 3D, 62/62 events). Combining labeled ORC with Mcm2–$7^{25quench}$ revealed a connection between ORC release and closing of the second Mcm2–7 ring. In the majority of events (47/54), the single ORC involved in helicase loading[8] was released at a time within experimental error of gate closure of the second Mcm2–7 (Fig. 3E). In the remaining events, ORC was retained on the DNA after second ring closure. Interestingly, relative to association of the second Mcm2–7, the average time until second Mcm2–7 ring closure was much longer than the previously determined average time until establishment of Mcm2–7-Mcm2–7 double-hexamer interactions (as measured by FRET between the N-termini of the first and second Mcm2–7[8], Supplementary Fig. 4E). Thus, an open second Mcm2–7 ring forms initial double-hexamer interactions with a closed first Mcm2–7 (Fig 3C), raising the possibility that the closed first Mcm2–7 ring could act as a template to facilitate closing of the second Mcm2–7. In combination, our data strongly suggest that ORC release only occurs after Mcm2–7 double-hexamer formation and closure of both Mcm2–7 rings, a mechanism that would ensure that ORC is retained until the completion of origin licensing.

Mcm2–7 ATP hydrolysis is required for Cdt1 release and ring closure

To further investigate the mechanism of Mcm2-Mcm5 gate closing, we asked if the ATPase activities of Mcm2–7, Cdc6, or ORC control this event. Based on the temporal connection

between gate closure and Cdt1 release, we focused on a mutation in the Mcm5-Mcm3 ATPase active site (*mcm5-R549A*, Supplementary Fig. 5A) that is defective for Cdt1 release and Mcm2–7 loading[13,14]. We incorporated this mutant into Mcm2–7^{25FRET} and monitored Mcm2-Mcm5 gate status. Strikingly, Mcm2–7$^{25FRET\text{-}5RA}$ remains in an open-gate (E_{FRET} ~0.18) state indefinitely after DNA association (Fig. 4A and Supplementary Fig. 5B). In contrast, using Cdc6[22] or ORC[15] ATPase mutants did not prevent Mcm2-Mcm5 gate closure (Fig. 4B). The kinetics of Cdc6 release were unchanged by Mcm2–7^{5RA} (Fig. 4C). In contrast, the dwell time of Cdt1 associated with Mcm2–7^{5RA} was dramatically extended relative to wild-type Mcm2–7 (Fig. 4D). In most cases (87/109), Cdt1-DNA association was as long as Mcm2–7^{5RA} association, including many long-lived associations that ended with the simultaneous release of Mcm2–7 and Cdt1 (e.g., Supplementary Fig. 5C), as expected if the lack of Cdt1 release prevented ring closure. Interestingly, we did not observe any second Mcm2–7 associations (0/109) for the Mcm2–7^{5RA} mutant, suggesting release of Cdt1 and/or ring closure must be completed prior to second Mcm2–7 recruitment.

Discussion

Our results support the initial conclusion that the E_{FRET} ~0.18 and ~0.36 states of Mcm2–7^{25FRET} represent the open and closed Mcm2-Mcm5 gate. The Mcm2–7 ring was in the E_{FRET} ~0.18 state before and immediately after DNA binding, consistent with an open Mcm2–7 ring allowing DNA access to the central channel. Similarly, all Mcm2–7$^{25FRET\text{-}5RA}$ DNA associations remained in the open (E_{FRET} ~0.18) state and were released by a high-salt wash that removes incompletely loaded Mcm2–7 (32/32 events[12,23]). Consistent with this conclusion, recent high-resolution cryo-EM structural studies of Mcm2–7 and Cdt1-Mcm2–7 found that both complexes are in an open-ring conformation[24]. The Mcm2–7 but not the ORC or Cdc6 ATPases are required for helicase loading[13,14]. Consistent with the higher E_{FRET} state reflecting a loaded, closed-ring Mcm2–7, the Mcm5-Mcm3 ATPase mutant, but not mutations in ORC or Cdc6 ATPases, prevented formation of this state. Future studies will be required to determine if other Mcm2–7 ATPase mutants have the same effect. Finally, attainment of the E_{FRET} ~0.36 state occurred independently for each Mcm2–7 complex, consistent with evidence that they are loaded one at a time [6–9]. Although structural studies of the loaded double-hexamer suggest show a completely closed Mcm2–7 ring[21], our findings do not exclude the possibility that the closed state we observe by FRET is sufficiently open to allow ssDNA to escape the loaded double-hexamer.

In addition to revealing the times of Mcm2–7 ring closure during helicase loading, the concomitant release of Cdt1 and closure of the Mcm2-Mcm5 gate and the inhibition of both events by the Mcm5-Mcm3 ATPase mutant support a model in which these events are causally linked (Fig. 5). We propose that the positively charged Mcm2–7 central channel and Cdt1 binding (Fig. 2C, Supplementary Table 3) favor an open conformation of the Mcm2–7 ring off the DNA. ORC–Cdc6 recruit an open Cdt1-Mcm2–7 ring such that it encircles DNA[7], similar to recent studies of archaeal Mcm loading[25]. Although Cdt1 binding was not required to maintain an open Mcm2–7 off DNA, we propose that Cdt1 holds the Mcm2–7 ring open after negatively-charged DNA binds to the positively-charged Mcm2–7 central channel. Finally, after Cdc6 is released, we propose that Mcm5-Mcm3 ATP hydrolysis (and perhaps other Mcm2–7 ATPases) stimulates Cdt1 release triggering Mcm2-Mcm5 gate

closure. It is also possible that Mcm5-Mcm3 ATP hydrolysis directly stimulates ring closure which causes Cdt1 release. Although ORC–Cdc6 has been proposed to function like a sliding-clamp loader during helicase loading[7], of the known sliding clamp functions[26], it appears this complex only retains the function of recruiting a protein-ring to the DNA. ORC and Cdc6 are not required to open the Mcm2–7 ring (Fig. 1 and 3) and ATP hydrolysis by ORC or Cdc6 is not required for ring closure (Fig. 4B). This does not eliminate other possible roles for ORC–Cdc6 including stimulating Mcm2–7 ATP hydrolysis[6] or altering Mcm2–7 conformation to facilitate ring closure[7].

The ordered release of Cdc6 and Cdt1 and the connection of the latter event to ring closure creates a window of time for Mcm2–7 loading quality control[13,14,17]. Cdc6 ATP hydrolysis is connected to the release non-productive Mcm2–7 complexes[13,14]. Because the Mcm2–7 ring is open throughout Cdc6 DNA association (Fig. 3D), this quality control mechanism would not require reopening of the Mcm2–7 ring. In addition, the ordered closure of rings would allow the first and second Mcm2–7 complexes to be assessed separately. Although the mechanism of this release is unclear, one simple hypothesis is that an ATP-dependent release of Cdc6 prior to Mcm2–7 ring closure leads to the simultaneous release of open non-productive Mcm2–7 complexes.

Our findings indicate that loading of the two Mcm2–7 complexes associated with origin licensing is the result of a single coordinated event rather than two independent Mcm2–7 loading events. Both the lack of second Mcm2–7 association for the Mcm2–7^{5RA} mutant and the finding that gate closure by the first Mcm2–7 always preceded DNA association of a second Mcm2–7 (Fig. 1B and S2A, 47/47 events), strongly suggest that recruitment of the second Mcm2–7 requires completion of the first loading event. This is inconsistent with models suggesting that two ORC molecules independently recruit and load one Mcm2–7. The connection between ORC release and closure of the second but not the first Mcm2–7 ring (Fig. 3E) also supports a coordinated mechanism. Importantly, these properties would ensure single Mcm2–7 loading events only occur as the first step in forming a Mcm2–7 double-hexamer.

The combination of fully reconstituted biochemical assays[27] and detailed structural models of key replication intermediates[7,9,21] has provided important insights into the events of eukaryotic replication initiation. Single-molecule studies complement these approaches by revealing reaction kinetics that are difficult to assay in asynchronous bulk reactions, identifying intermediates that are too short-lived or dynamic to analyze structurally and by monitoring changes in protein conformation in real time. Our findings show how the combination of single-molecule colocalization and single-molecule FRET can elucidate the complex and coordinated protein dynamics of helicase-loading events. More importantly, our findings reveal features of origin licensing that can reduce incomplete or incorrect events and, therefore, improve genome stability.

Methods

Protein expression and purification strains

Cdc6^{SORT549} (pET-GSS-Cdc6), Cdt1^{SORT549}–Mcm2–7^{4SNAP} (yST166) and ORC^{1SORT549} (yST163) were purified as described previously[8]. To monitor the Mcm2-Mcm5 gate, Cdt1–Mcm2–7^{25FRET} expressing strains were constructed by introducing an Asc I site after amino acid 721 of Mcm2 and amino acid 591 of Mcm5[2]. A SNAP- (Mcm5, NEB) or CLIP-tag (Mcm2, NEB) was inserted with 10 amino acid linkers (GGSGGSGGSG) at each junction. To purify Mcm2–7^{25FRET}, Mcm2–721^{CLIP} and Mcm5–591^{SNAP} were expressed in conjunction with the remaining wild-type Mcm2–7 subunits and Cdt1 (yST229) or in the absence of Cdt1 (yST266, to make Mcm2–7$^{25FRET\text{-}biotin}$) and labeled with CLIP-Surface™ 647(NEB) and SNAP-Surface™ 549 (NEB) as described below. To monitor gate closure by quenching (Mcm2–7^{25quench}) or to create an alternate Mcm2-Mcm5 gate FRET pair (Mcm2–7^{2C5FRET}), Mcm2^{SORT} (Mcm2 with LPETGG at its C-terminus) and Mcm5–591^{SNAP} were co-expressed with the remaining wild type Mcm2–7 subunits and Cdt1 (yST220). Sortase was used to attach Mcm2^{SORT} to the peptide NH_2-GGGHH HHHHH HHHC-COOH coupled to maleimide-Dy549 and Mcm5–591^{SNAP} was coupled to SNAP-BHQ-2 to form Mcm2–7^{25quench} (see below) or SNAP- Surface™ 649 to form Mcm2–7^{2C5FRET}. Mcm2-Mcm5 gate FRET was monitored in the context of the Mcm5-R549A mutant protein by incorporating the mutation into Mcm5 subunit of the Cdt1–Mcm2–7^{25FRET} expressing strain (yST299). The resulting mutant Cdt1-Mcm2–7 was labeled as described for Mcm2–7^{25FRET} to form Mcm2–7$^{25FRET\text{-}mcm5RA}$. The effect of Mcm5-R549A on Cdt1 release was monitored by purifying Cdt1-Mcm2–7 from a strain expressing Mcm5-R549A, Mcm4^{SNAP}, Cdt1^{SORT} and the remaining wild-type Mcm subunits (yST291). Mcm4^{SNAP} was labeled with SNAP-JF646 (gift of Luke Lavis, Janelia Research Campus) and Cdt1^{SORT} was coupled to the peptide NH_2-GGGHH HHHHH HHHC-COOH coupled to maleimide-Dy549 to make Cdt1SORT549–Mcm2–7$^{4SNAP\text{-}mcm5RA}$. The effect of Mcm5-R549A on Cdc6 release was monitored by purifying Cdt1–Mcm2–7 from a strain expressing Mcm5-R549A, Mcm4^{SNAP}, Cdt1 and the remaining wild-type Mcm subunits (yST289) to make Cdt1–Mcm2–7^{4SNAP_mcm5RA}.

Purification and Fluorescent Labeling of Cdt1–Mcm2–7

S. cerevisiae (W303 background) strains yST229, yST220, yST299 or yST291 were grown to OD_{600} = 1.2 in 8 liters of YEP supplemented with 2% glycerol (v/v) at 30°C. Addition of 2% galactose (w/v) and α-factor (100 ng/mL) induced Cdt1-Mcm2–7 expression and arrested cells at G1. After 6 hours cells were harvested and sequentially washed with 50 ml of ice-cold MilliQ water with 0.2 mM PMSF followed by 150 ml buffer A (50 mM HEPES-KOH pH [7.6], 5 mM MgOAc, 1 mM ZnOAc, 2 mM ATP, 1 mM DTT, 10% glycerol, 0.02% NP-40) supplemented with 0.1 mM EDTA, 0.1 mM EGTA, 0.75 M potassium glutamate (KGlu) and 0.8 M Sorbitol. The washed pellet was resuspended in approximately 1/3 of packed cell volume of buffer A containing 0.1 mM EDTA, 0.1 mM EGTA, 0.75 M KGlu, 0.8 M Sorbitol, Complete Protease Inhibitor Cocktail Tablet (1 tablet per 15 mL total volume; Roche) and frozen dropwise in liquid nitrogen. Frozen cells were lysed in a SamplePrep freezermill (SPEX) and the lysate was clarified by ultracentrifugation in Type 70 Ti rotor at 45 krpm for 90 min at 4°C. The supernatant was applied to 2 ml anti-M2

FLAG resin (Sigma) pre-equilibrated in buffer A containing 0.1 mM EDTA, 0.1 mM EGTA and 0.75 M KGlu and incubated with rotation for 3 hours at 4°C. The resin was collected on a column and the flow-through was discarded. The resin was washed with 20 ml of buffer A with 0.3 M KGlu. Cdt1-Mcm2–7 was eluted with buffer A containing 0.3 M KGlu and 0.15 mg/mL 3xFLAG peptide. Peak fractions containing Cdt1-Mcm2–7 were pooled, and the protein was concentrated to ~ 1 mg/mL using a Vivaspin 6 centrifugal concentrator (molecular weight cutoff = 100 kDa, Sartorius) and aliquoted into 0.8 mL fractions. Starting with 8 L of cells, the yield is typically 2 mg of 95% pure Sort-Cdt1–Mcm2–7, according to SDS-PAGE.

SNAP or CLIP-tagged Cdt1-Mcm2–7 ($Cdt1^{SORT}$–$Mcm2–7^{4SNAP}$, Cdt1–$Mcm2–7^{2C5FRET}$ or Cdt1–$Mcm2–7^{25FRET}$) was labeled with SNAP-Surface™ 549 (NEB; Dy549), SNAP-BHQ-2, SNAP-JF646 (gift of Luke Lavis, Janelia Research Campus) or CLIP-Surface™ 647 by incubating with 1 nmol of dye at room temperature for 1hr. To make $Mcm2–7^{25FRET\text{-}biotin}$, SNAP-549-biotin was substituted for SNAP-Surface™ 549. For SORT-tagged Cdt1-Mcm2–7 ($Cdt1^{Sort}$ –$Mcm2–7^{4SNAP}$, Cdt1–$Mcm2–7^{2C5FRET}$ or Cdt1–$Mcm2–7^{25quench}$), 1 mg of Cdt1-Mcm2–7 was incubated with equimolar amount of Srt5° evolved sortase[28], purification described below) and $CaCl_2$ was added to a final concentration of 5 mM in buffer A with 0.3 M KGlu. This was mixed with 100 nmol of peptide carrying a Sort-tag and labeled with Dy549 (Dyomics), dissolved in 200 μL of buffer A with 0.3 M KGlu (sequence and fluorescent labeling of the peptide are described below). The reaction was incubated at room temperature for 15 min, and then quenched with 20 mM EDTA. The net result of the sortase reaction is coupling of the fluorescently-labeled (or biotinylated) peptide to the N-terminus of Cdt1 with the sequence NH2-CHHHHHHHHHHLPETGGG followed by the remainder of the protein or to the C-terminus of Mcm2 with the sequence LPETGGGHHHHHHHHHHC-COOH.

For SNAP or CLIP-tagged Cdt1-Mcm2–7, after coupling the proteins to fluorophore(s), the reaction was applied to a Superdex 200 10/300 gel filtration column equilibrated in buffer A with 0.1 mM EDTA, 0.1 mM EGTA, and 0.3 M KGlu. Peak fractions containing Cdt1-Mcm2–7 were pooled, aliquoted and stored at −80°C.

For SORT-tagged Cdt1-Mcm2–7, after dye-coupling, the reaction was applied to a Superdex 200 10/300 gel filtration column equilibrated in buffer A with 0.1 mM EDTA, 0.1 mM EGTA, 0.3 M KGlu, and 10 mM imidazole. Peak fractions containing peptide-coupled Cdt1-Mcm2–7 were pooled and incubated with 0.5 mL of cOmplete His-Tag Purification Resin (Roche) pre-equilibrated in buffer A with 0.1 mM EDTA, 0.1 mM EGTA, 0.3 M KGlu, 10 mM imidazole, for 1 hour with rotation at 4°C. The flow-through was discarded and the resin was washed with 5 ml buffer A with 0.1 mM EDTA, 0.1 mM EGTA, 0.3 M KGlu and 10 mM imidazole. Peptide-coupled Cdt1-Mcm2–7 was eluted using buffer A with 0.1 mM EDTA, 0.1 mM EGTA, 0.3 M KGlu and 0.3 M imidazole. Peak fractions were pooled, aliquoted, and stored at −80°C.

Special note on handling of fluorescent dyes: light sources on all chromatography apparatuses (AKTA FPLC, HPLC) were turned off during preparative runs. Fractions

containing fluorescently-labeled peptides and proteins were determined during previous analytical runs.

Fluorescently-labeling of peptides for Sortase coupling, as well as purification of the Sortase A pentamutant enzyme and Ulp1 were performed as reported previously[8].

Percent labeling of Mcm2–7^{25FRET}

To determine the labeling efficiency of the SNAP and CLIP tag labeling approaches in the MCM2–7^{25FRET} context, we purified and labeled Mcm2–7^{25FRET} with SNAP-Surface™ 549 and CLIP-Surface™ 647 on the Mcm5 and Mcm2 subunits, respectively. We imaged a standard reaction containing 0.25nM ORC, 1nM Cdc6 and 2.5nM Cdt1–Mcm2–7^{25FRET} using the described protocol and monitored colocalization of Mcm2–7^{25FRET} fluorescence with DNA fluorescence (to ensure that we were monitoring fully assembled complexes). Each colocalization was scored as exhibiting both D and A fluorescence, only D, or only A. By assuming that the labeling reactions of the SNAP and CLIP tags in Mcm2–7^{25FRET} were independent, we calculated from the observed D and A colocalization frequencies that SNAP labeling efficiency was ~74%, and CLIP labeling efficiency was ~81%, yielding ~60% of Mcm2–7^{25FRET} complexes with both D and A fluorophores.

Synthesis of SNAP-549-Biotin and SNAP-BHQ2

Commercially available compounds were used without further purification. Reaction yields were not optimized. Reversed-phase high-performance liquid chromatography (HPLC) was performed on Agilent LC-MS Single Quad System 1200 Series (analytical) and Agilent 1100 Preparative-scale Purification System (semi-preparative). Analytical HPLC was performed on Waters Atlantis T3 C18 column (2.1 × 150 mm, 5 μm particle size) at a flow rate of 0.5 mL/min with a binary gradient from Phase A (0.1 M triethyl ammonium bicarbonate (TEAB) or 0.1% trifluoroacetic acid (TFA) in water) to Phase B (acetonitrile) and monitored by absorbance at 280 nm. Semi-preparative HPLC was performed on VYDAC 218TP series C18 polymeric reversed-phase column (22 × 250 mm, 10 μm particle size) at a flow rate of 20 mL/min. Mass spectra were recorded by electrospray ionization (ESI) on an Agilent 6120 Quadrupole LC-MS or on an Agilent 6210 Time-of-Flight (TOF) or on a Thermo Scientific QExactive system.

SNAP-BHQ2 (BG-BHQ2, Supplementary Fig. 6A) was prepared by reacting the building block BG-NH_2 (NEB) with commercially available BHQ-2 Succinimidyl ester (LGC Biosearch) as described (*23*). BHQ-2 Succinimidyl ester (2.5 mg, 4.1 μmol) was dissolved in anhydrous DMF (1.0 mL). BG-NH_2 (1.1 mg, 4.1 μmol) and triethylamine (0.56 μL, 4.1 μmol) were added and the reaction mixture stirred overnight at room temperature. The solvent was removed under vacuum and the product purified by reversed-phase HPLC using 0.1 M TEAB/acetonitrile gradient (yield = 21%). BG-BHQ2: ESI-MS *m/z* 759.3104 $[M+H]^+$ (calc. for $C_{38}H_{38}N_{12}O_6$, *m/z* 759.3110).

The bifunctional SNAP-549-Biotin (BG-549-biotin, Supplementary Fig. 6B) substrate was prepared by successive couplings of commercially available α-*N*-Fmoc-ε-*N*-Dde-lysine (Merck KGaA) with BG-NH_2 (NEB), *N*-(+)-biotin-6-aminocaproic acid *N*-succinimidyl ester (Sigma-Aldrich) and DY-549 acid (Dyomics) according to synthetic route described by

Kindermann et al[29] and Smith et al[30]. SNAP-549-Biotin was synthesized as follows: BG-NH_2 (250.0 mg, 0.92 mmol) was dissolved in anhydrous DMF (8 mL). HBTU (*N,N,N′,N′*-Tetramethyl-O-(1H–benzotriazol-1-yl)uronium hexafluorophosphate) (368.0 mg, 0.97 mmol), triethylamine (135 μL, 0.97 mmol), and Fmoc-Lys(Dde)-OH (515.5 mg, 0.97 mmol) were added and the reaction mixture stirred overnight at room temperature. The reaction mixture was poured onto water (80 mL). The white solid was collected by filtration, washed twice with water, and dried in desiccator under vacuum overnight (yield = 91%). BG-Lys(Dde)-Fmoc (8.0 mg, 10.2 μmol) was dissolved in anhydrous in DMF (1 mL). Et_2NH (3.2 μL, 30.9 μmol) was added and the reaction mixture stirred overnight at room temperature. The solvent was removed under vacuum. Crude BG-Lys(Dde)-NH_2 was dissolved in anhydrous DMF (1 mL). *N*-(+)-biotin-6-aminocaproic acid NHS (2.9 mg, 6.4 μmol) and triethylamine (1.0 μL, 7.0 mmol) were added and the reaction mixture stirred 1 h at room temperature. Reaction completion was monitored by LC-MS. A 2% solution of hydrazine in DMF (0.5 mL) was added and the reaction mixture stirred for 1 h at room temperature. The solvent was removed under vacuum and the product purified by reversed-phase HPLC using 0.1% TFA in water/acetonitrile gradient (yield = 76%). BG-Lys(NH_2)-Biotin: ESI-TOFMS *m/z* 738.3 $[M+H]^+$ (calcd. for $C_{35}H_{51}N_{11}O_5S$, *m/z* 738.4). BG-Lys(NH_2)-Biotin·TFA salt (2.3 mg, 2.7 μmol) was dissolved in anhydrous DMF (1 mL). DY-549 acid (2.7 mg, 3.0 μmol), HBTU (1.2 mg, 3.0 μmol) and triethylamine (0.6 μL, 4.5 μmol) were added and the reaction mixture stirred 1 h at room temperature. The solvent was removed under vacuum and the product purified by reversed-phase HPLC using 0.1 M TEAB/acetonitrile gradient (yield = 78%). BG-549-PEG-Biotin: ESI-TOFMS *m/z* 767.7552 $[M-2H]^{2-}$ (calc. for $C_{68}H_{91}N_{13}O_{18}S_5$, *m/z* 767.7532).

Single-Molecule Microscopy

The micro-mirror total internal reflection (TIR) microscope used for multiwavelength single-molecule using excitation wavelengths 488, 532, and 633 nm has been previously described[31,32]. Biotinylated AlexFluor488-labeled 1.3kb-long DNA molecules containing an origin were coupled to the surface of a reaction chamber through streptavidin. Briefly, the chamber surface was cleaned and derivatized using a 200:1 ratio of silane-NHS-PEG and silane-NHS-PEG-biotin[8]. We identified DNA molecule locations by acquiring 4–7 images with 488 nm excitation at the beginning of the experiment. Unless otherwise noted, helicase loading reactions contained 0.5nM ORC, 2nM Cdc6 and 5nM Cdt1–Mcm2–7. Reaction buffer was as previously described[13] except without any glycerol and with the addition of 2 mM dithiothreitol, 2 mg/ml bovine serum albumin (EMD Chemicals; La Jolla, CA), and an oxygen scavenging system (glucose oxidase and catalase) to minimize photobleaching[32]. After addition of protein to the DNA-coupled chamber, frames of one second duration were acquired. DNA was imaged before and immediately after adding the reaction to the slide but not throughout the experiment. The imaging protocol alternated between 1 s frames with the 532 laser on and 1 s frames with the 633 laser on over 20–30 minutes. Apparent E_{FRET} was calculated as described[33].

Because the events observed on each DNA molecule represent a independent measurement of the events being studied, all of the analyses evaluate many biological replicates.

Tethering of Mcm2–7 complexes

Tethering experiments were done using Mcm2–7$^{25FRET\text{-}biotin}$ in the absence of Cdt1 or Cdt1-biotin with Mcm2–7^{25FRET} purified in the absence of Cdt1. Complexes were added to the slide at a concentration of 0.04nM and coupling was briefly visualized. Free complexes were washed out using H-300mM KGlut, and imaged for 2 minutes by alternating between 1s frames with the 532 laser on, and 1s frames with the 633 laser on. Only complexes containing both 549 and 647 dyes were used for background subtraction and E_{FRET} calculations.

Single-molecule data analysis

Analysis of the CoSMoS data sets was similar to[34]. Specifically, we typically followed these four steps[35]: (1) defining the spatial relationship between the two images created at different excitation and emission wavelengths from the single field of view by the dual-view optical system (“mapping”), (2) correcting the data set for stage drift that occurred during the experiment (“drift correction”), (3) imaging the label on origin-DNA to identify the locations of single DNA molecules on the surface, and (4) integration of fluorescence emission from small regions centered at the pre-defined locations of coupled DNA locations in each acquired image to obtain plots of fluorescence intensity vs. time. These steps were carried out using custom image-processing software (https://github.com/gelles-brandeis/CoSMoS_Analysis) implemented in MATLAB (The Mathworks, Natick, MA). Confidence intervals for kinetic data were determined by bootstrapping.

Both the dual imaging optics and chromatic aberrations result in spatial displacement between fluorescent spot images of co-localized species that are labeled with different color dyes. Accurate co-localization of the differentially-labeled species therefore requires use of a mapping procedure. For each pair of colors a list of several hundred reference spot pairs were collected using a sample containing a surface-tethered oligonucleotide that was labeled with Alexa488, Cy3 and Cy5. Mapping the coordinates of a fluorescent spot to the equivalent location at a different color was performed using a transformation with fit parameters based on just the 15 nearest reference spots[35].Drift correction and spot-detection were carried out as described in[35]. Fluorescence emission from labeled complexes was integrated over a 0.37 μm^2 area centered at each drift corrected origin-DNA location, yielding for each DNA molecule a separate intensity time course for each color of fluorescent label being observed.

FRET and quenching data analysis

Images containing spots that were analyzed to produce a FRET time course were first mapped and drift-corrected (see above). By alternating between their laser excitation wavelengths we monitored the co-localization of donor and acceptor-labeled Mcm2–7 hexamers with the origin-DNA molecule. To determine the time until formation of the E_{FRET} ~0.36 state, we noted the earliest time point at which the E_{FRET} values increased by either 0.15 for the 1st Mcm2–7 or 0.1 for the 2nd Mcm2–7. Only Mcm2–7 molecules that were labeled with both fluorophores were used for analysis of the first Mcm2–7. For analysis of the second Mcm2–7, both the first and the second Mcm2–7 molecules had to be labeled with both fluorophores.

To calculate apparent FRET efficiencies, the baseline for each fluorescence intensity trace was first subjected to a low pass filter. That smoothed baseline was then subtracted from the starting trace, resulting in a fluorescence time record with a zero mean baseline[31] (e.g. Figure 1B, panels i and ii). Apparent FRET efficiency was calculated using

$E_{\mathrm{FRET}}=\frac{I_{\mathrm{Acceptor}}}{I_{\mathrm{Acceptor}}+I_{\mathrm{Donor}}}$ where I_{Acceptor} and I_{Donor} are the acceptor and donor emission intensities observed during donor excitation, respectively. No gamma correction was applied because no systematic change in (I_{Acceptor} + I_{Donor}) was observed upon changes in E_{FRET} (e.g., Fig. 1B, S2A) or upon acceptor photobleaching.

E_{quench} was calculated on baseline-corrected data (of single Mcm2–7 molecules) as described in Supplementary Fig. 4D.

Measuring FRET values for soluble Mcm2–7$^{25\mathrm{FRET}}$

To generate sufficient loaded Mcm2–7$^{25\mathrm{FRET}}$, a large-scale helicase-loading reaction was performed with 20 pmoles of bead-attached, origin DNA 80 pmoles of Mcm2–7$^{25\mathrm{FRET}}$, 20 pmoles of ORC and 40 pmoles of Cdc6[13]. After a 20 minute incubation, the DNA beads were washed with a high-salt buffer (to remove incompletely loaded protein) and loaded Mcm2–7$^{25\mathrm{FRET}}$ was released from beads by DNAse I treatment as previously described[13]. The released, loaded Mcm2–7$^{25\mathrm{FRET}}$ or a similar concentration of unloaded solution Cdt1–Mcm2–7$^{25\mathrm{FRET}}$ were placed in a cuvette and excited at 549 nm. Flourescence emission was detected from 560 nm to 690 nm and the peak values of donor (574 nm) and acceptor (670 nm) emission were used to determine E_{FRET} values. Reported uncertainties are the standard deviations of four separate experiments.

Statistical analysis

Confidence intervals (C.I.) were determined using bootstrapping with either 1000 samples (Figs. 2, 4 and Supplementary Figs. 4 and 5) or 250 samples (Supplementary Tables).

Supplementary Material

Refer to Web version on PubMed Central for supplementary material.

Acknowledgments

We are grateful to the members of the Bell laboratory for useful discussions, Bob Sauer for comments on the manuscript, and Luke D. Lavis (Janelia Research Campus) for providing Janelia Fluorophores. This work was supported by NIH grants R01 GM52339 (S.P.B.) and R01 GM81648 (J.G.) and a grant from the G. Harold and Leila Y. Matthews Foundation (J.G.). S.T. was supported in part by an NIH Pre-Doctoral Training Grant (GM007287). S.P.B. is an investigator with the Howard Hughes Medical Institute. This work was supported in part by the Koch Institute Support Grant P30-CA14051 from the NCI. We thank the Koch Institute Swanson Biotechnology Center for technical support, specifically the Biopolymers and Genomics cores.

References

1. Yardimci H, Walter JC. Prereplication-complex formation: a molecular double take? Nat Struct Mol Biol. 2014; 21:20–25. [PubMed: 24389553]
2. Samel SA, et al. A unique DNA entry gate serves for regulated loading of the eukaryotic replicative helicase MCM2–7 onto DNA. Genes Dev. 2014; 28:1653–1666. [PubMed: 25085418]

3. Bochman ML, Schwacha A. The Mcm2–7 complex has in vitro helicase activity. Mol Cell. 2008; 31:287–293. [PubMed: 18657510]
4. Remus D, et al. Concerted Loading of Mcm2–7 Double Hexamers around DNA during DNA Replication Origin Licensing. Cell. 2009; 139:719–730. [PubMed: 19896182]
5. Aparicio OM, Weinstein DM, Bell SP. Components dynamics of DNA replication complexes in S. cerevisiae: redistribution of MCM proteins and Cdc45p during S phase. Cell. 1997; 91:59–69. [PubMed: 9335335]
6. Fernández-Cid A, et al. An ORC/Cdc6/MCM2–7 complex is formed in a multistep reaction to serve as a platform for MCM double-hexamer assembly. Mol Cell. 2013; 50:577–588. [PubMed: 23603117]
7. Sun J, et al. Cryo-EM structure of a helicase loading intermediate containing ORC-Cdc6-Cdt1-MCM2–7 bound to DNA. Nat Struct Mol Bio. 2013; 20:944–951. [PubMed: 23851460]
8. Ticau S, Friedman LJ, Ivica NA, Gelles J, Bell SP. Single-molecule studies of origin licensing reveal mechanisms ensuring bidirectional helicase loading. Cell. 2015; 161:513–525. [PubMed: 25892223]
9. Sun J, et al. Structural and mechanistic insights into Mcm2–7 double-hexamer assembly and function. genesdev.cshlp.org.
10. Evrin C, et al. A double-hexameric MCM2–7 complex is loaded onto origin DNA during licensing of eukaryotic DNA replication. Proc Natl Acad Sci USA. 2009; 106:20240–20245. [PubMed: 19910535]
11. Bell SP, Stillman B. ATP-dependent recognition of eukaryotic origins of DNA replication by a multiprotein complex. Nature. 1992; 357:128–134. [PubMed: 1579162]
12. Randell JCW, Bowers JL, Rodríguez HK, Bell SP. Sequential ATP hydrolysis by Cdc6 and ORC directs loading of the Mcm2–7 helicase. Mol Cell. 2006; 21:29–39. [PubMed: 16387651]
13. Kang S, Warner MD, Bell SP. Multiple Functions for Mcm2–7 ATPase Motifs during Replication Initiation. Mol Cell. 2014; 55:655–665. [PubMed: 25087876]
14. Coster G, Frigola J, Beuron F, Morris EP, Diffley JFX. Origin licensing requires ATP binding and hydrolysis by the MCM replicative helicase. Mol Cell. 2014; 55:666–677. [PubMed: 25087873]
15. Bowers JL, Randell JCW, Chen S, Bell SP. ATP hydrolysis by ORC catalyzes reiterative Mcm2–7 assembly at a defined origin of replication. Mol Cell. 2004; 16:967–978. [PubMed: 15610739]
16. Chang F, et al. Cdc6 ATPase activity disengages Cdc6 from the pre-replicative complex to promote DNA replication. eLife. 2015; 4:1–42.
17. Frigola J, Remus D, Mehanna A, Diffley JFX. ATPase-dependent quality control of DNA replication origin licensing. Nature. 2013; 495:339–343. [PubMed: 23474987]
18. Deegan TD, Diffley JF. MCM: one ring to rule them all. Curr Opin Struct Biol. 2016; 37:145–151. [PubMed: 26866665]
19. Costa A, et al. The structural basis for MCM2–7 helicase activation by GINS and Cdc45. Nat Struct Mol Biol. 2011; 18:471–477. [PubMed: 21378962]
20. Lyubimov AY, Costa A, Bleichert F, Botchan MR, Berger JM. ATP-dependent conformational dynamics underlie the functional asymmetry of the replicative helicase from a minimalist eukaryote. Proc Natl Acad Sci USA. 2012; 109:11999–12004. [PubMed: 22778422]
21. Li N, et al. Structure of the eukaryotic MCM complex at 3.8 Å. Nature. 2015; 524:186–191. [PubMed: 26222030]
22. Schepers A, Diffley JF. Mutational analysis of conserved sequence motifs in the budding yeast Cdc6 protein. J Mol Biol. 2001; 308:597–608. [PubMed: 11350163]
23. Donovan S, Harwood J, Drury LS, Diffley JF. Cdc6p–dependent loading of Mcm proteins onto pre-replicative chromatin in budding yeast. Proc Natl Acad Sci USA. 1997; 94:5611–5616. [PubMed: 9159120]
24. Zhai Y, et al. Open-ringed Structure of the Cdt1-MCM2–7 Complex as a Precursor of the MCM Double Hexamer. Nat Struct Mol Biol. in press.
25. Samson RY, Abeyrathne PD, Bell SD. Mechanism of Archaeal MCM Helicase Recruitment to DNA Replication Origins. Mol Cell. 2016; 61:287–296. [PubMed: 26725007]
26. Kelch BA. Review: The lord of the rings: Structure and mechanism of the sliding clamp loader. Biopolymers. 2016; 105:532–546. [PubMed: 26918303]

27. Yeeles JTP, Deegan TD, Janska A, Early A, Diffley JFX. Regulated eukaryotic DNA replication origin firing with purified proteins. Nature. 2015; 519:431–435. [PubMed: 25739503]

Methods-only references

28. Chen I, Dorr BM, Liu DR. A general strategy for the evolution of bond-forming enzymes using yeast display. Proc Natl Acad Sci USA. 2011; 108:11399–11404. [PubMed: 21697512]

29. Kindermann M, Sielaff I, Johnsson K. Synthesis characterization of bifunctional probes for the specific labeling of fusion proteins. Bioorg Med. Chem. Lett. 2004; 14:2725–2728. [PubMed: 15125922]

30. Smith BA, et al. Three-color single molecule imaging shows WASP detachment from Arp2/3 complex triggers actin filament branch formation. eLife. 2013; 2:e01008. [PubMed: 24015360]

31. Friedman LJ, Gelles J. Mechanism of transcription initiation at an activator-dependent promoter defined by single-molecule observation. Cell. 2012; 148:679–689. [PubMed: 22341441]

32. Friedman LJ, Chung J, Gelles J. Viewing dynamic assembly of molecular complexes by multi-wavelength single-molecule fluorescence. Biophys. J. 2006; 91:1023–1031. [PubMed: 16698779]

33. Crawford DJ, Hoskins AA, Friedman LJ, Gelles J, Moore MJ. Single-molecule colocalization FRET evidence that spliceosome activation precedes stable approach of 5' splice site and branch site. Proc Natl Acad Sci USA. 2013; 110:6783–6788. [PubMed: 23569281]

34. Hoskins AA, et al. Ordered and dynamic assembly of single spliceosomes. Science. 2011; 331:1289–1295. [PubMed: 21393538]

35. Friedman LJ, Gelles J. Multi-wavelength single-molecule fluorescence analysis of transcription mechanisms. Methods. 2015; 86:27–36. [PubMed: 26032816]

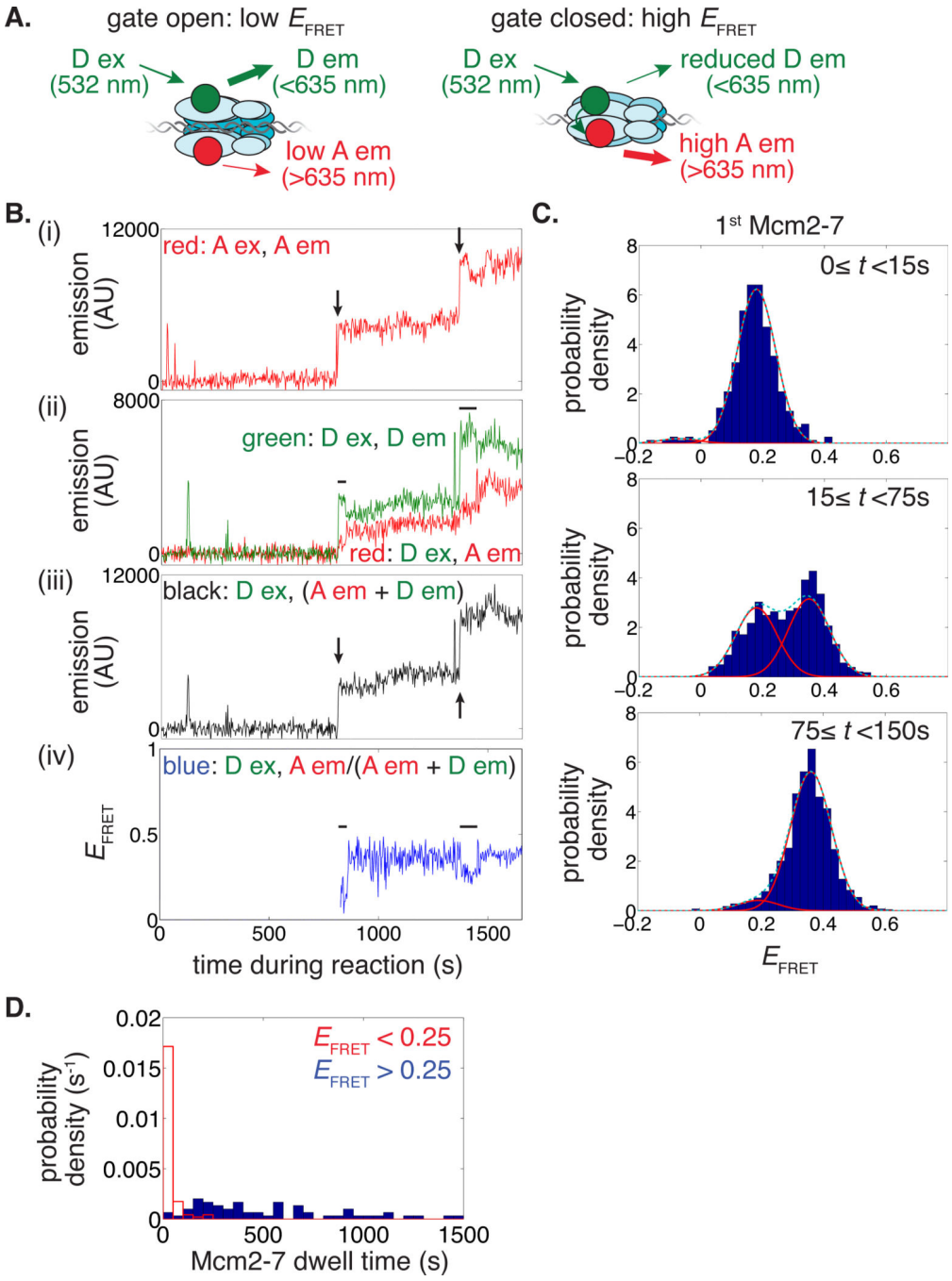

Figure 1. Mcm2–7 hexamers associate with DNA in an open-gate conformation and subsequently close

(A) Schematic of DNA-bound Mcm2–7^{25FRET} in the gate-open and gate-closed states. Mcm2 and Mcm5 are labeled with acceptor (A, red circle) and donor (D, green circle) fluorophores, respectively. Mcm2-Mcm5 gate closure increases proximity of the fluorophores and FRET efficiency (E_{FRET}). Fluorescence excitation (ex) and emission (em) wavelengths are indicated.

(B) Example recording of Mcm2–7^{25FRET} associating with origin DNA. Acceptor-excited (i, A ex, A em) and donor-excited (ii, D ex, D em and D ex, A em) emission records are shown

together with calculated donor-excited total emission (iii) and E_{FRET} (iv). Black arrows show initial association of long-lived Mcm2–7^{25FRET}. Black bars highlight low E_{FRET} intervals observed at the beginning of these associations.

(C) Histograms of EFRET values recorded during the indicated time intervals after association of the first Mcm2–7^{25FRET} with origin DNA. Fits to the sum (dashed cyan) of two Gaussians (red) yielded fit parameters reported in Supplementary Table 1. For accurate E_{FRET} determination, only the 51 first Mcm2–7 associations that retained D and A fluorophores for >150s and that lacked a second Mcm2–7 association within 150s of DNA association were analyzed. The same molecules are used for each histogram with data from 255 (0–15s), 1020 (15–75s) and 1320 (75–150s) total time points plotted.

(D) Histogram of single Mcm2–7 dwell times plotted as a probability density. Mcm2–7 associations with a time-averaged E_{FRET} <0.25 (N=91 molecules) are plotted in red and those with a time-averaged E_{FRET} >0.25 (N=59 molecules) in blue. Time-averaged E_{FRET} was calculated over the duration of the association or until a second Mcm2–7 associated. For 29 molecules with average E_{FRET} >0.25 the measured dwell times were truncated by the end of the recording.

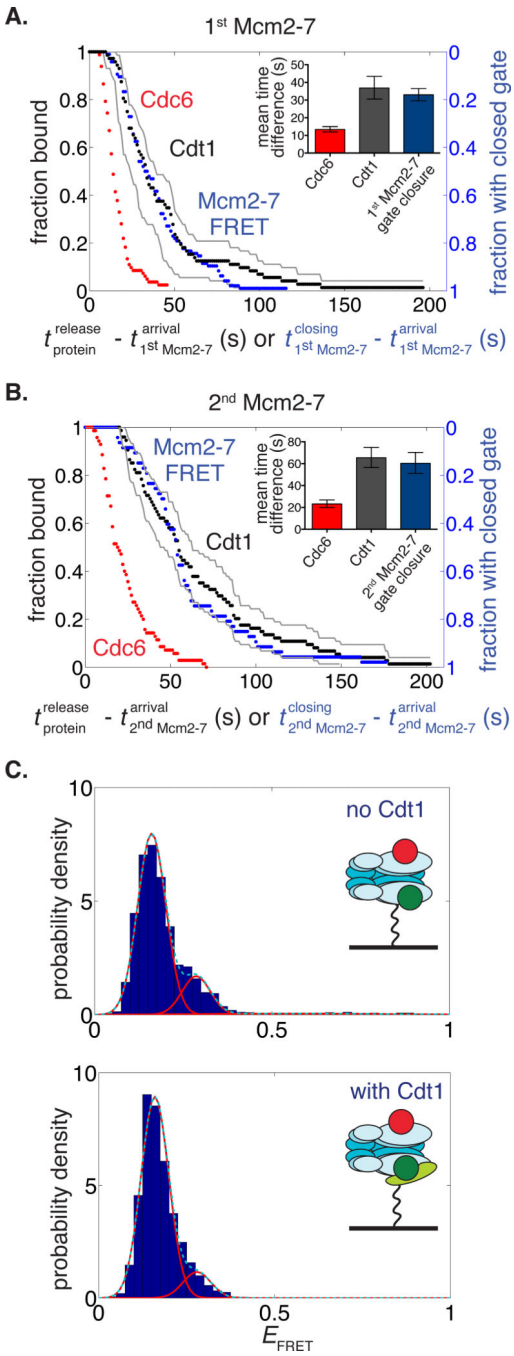

Figure 2. Mcm2–7 gate closing correlates with Cdt1 release on DNA but not free in solution

(A) Fraction of dye-labeled Cdc6 (blue, N=96 molecules) or Cdt1 (black, N=72 molecules) association retained at various times after first Mcm2–7 association (from ref. 8, left scale) are plotted compared to times of first Mcm2–7^{25FRET} gate closure (blue, right scale, N=96 molecules). The 95% confidence interval (C.I.) around the time of Cdt1 release is shown in grey. Inset shows mean release times or gate closure times (± 95% C.I.s). Gate closure times were based on the first time point at which the E_{FRET} value increased by 0.15 over the average of five previous time points and was sustained at least five time points.

(B) The same plots as in (A) are shown for events after association of the second Mcm2–7^{25FRET}. Gate closure is shown in blue (N=47 molecules) on the right scale. Release of Cdc6 (red; N=70 molecules) and Cdt1 (from ref. 8, black; N=74 molecules; 95% C.I. in gray) on the left scale. Gate closure times were determined as in (A) except the E_{FRET} increase threshold was 0.1.

(C) Histograms of E_{FRET} values of tethered Mcm2–7^{25FRET} either in the absence (N=32 molecules, 2014 total time points) or presence (N=60 molecules, 3712 total time points) of Cdt1 were fit with the sum (cyan) of two (with Cdt1) or three (no Cdt1) Gaussians (red) yielding the fit parameters reported in Supplementary Table 3. The presence of Cdt1 moderately increased the percentage of the data in the open (E_{FRET} ~0.16) state (88% v. 80%). In both cases, the majority of the remaining data fit to a second E_{FRET} ~0.28 state, likely representing a partially closed Mcm2-Mcm5 gate. Insets show schemes of attachment. Mcm2–7^{25FRET} was tethered to the slide surface either directly through the Mcm5 subunit (no Cdt1, Mcm2–$7^{25FRET\text{-}biotin}$) or indirectly through biotinylated Cdt1 tethered to the surface (with Cdt1).

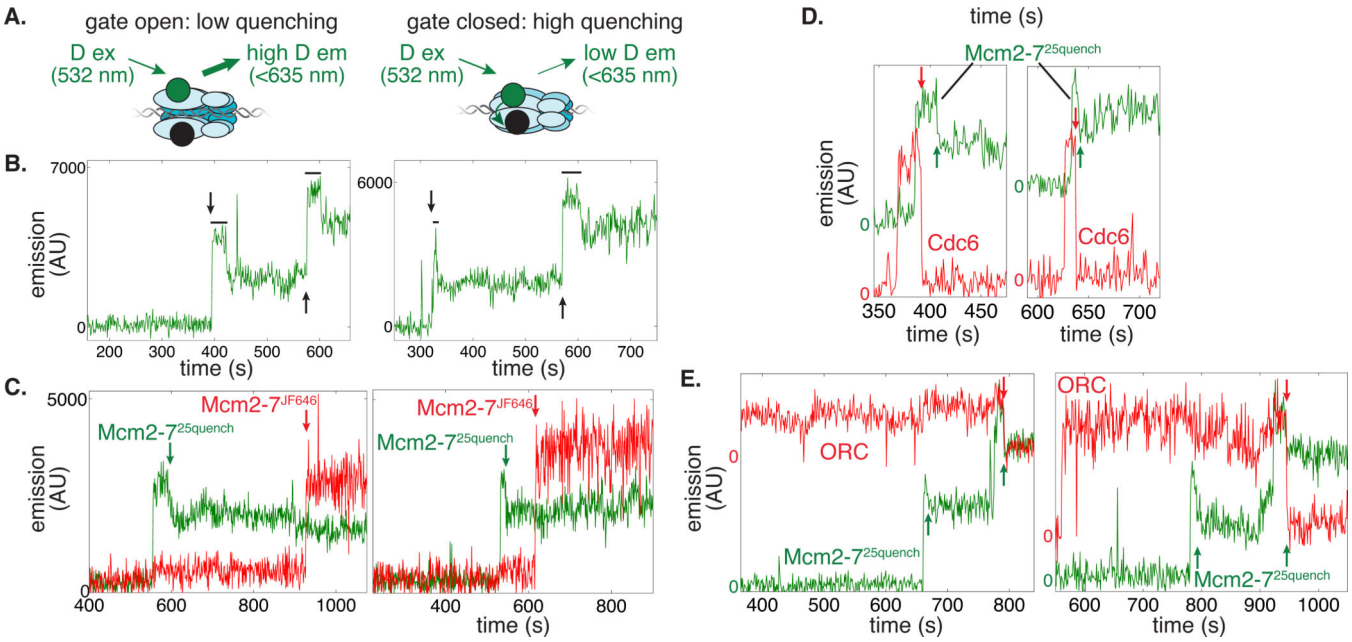

Figure 3. Closure of the second Mcm2–7 ring correlates with ORC release

(A) Schematic of Mcm2–7^{25quench} labeling in the gate-open and gate-closed states. Mcm2 and Mcm5 were labeled with donor fluorophore (D, green circle) and quencher (BHQ-2, black circle), respectively. Mcm2-Mcm5 gate closure increases proximity of the fluorophore and quencher, decreasing D em.

(B) Two example recordings of sequential association of two Mcm2–7^{25quench} molecules associating with individual origin DNA molecules. Black arrows show initial association of long-lived Mcm2–7^{25quench}. Black bars highlight intervals of no or low quenching following the first and second Mcm2–7^{25quench} associations.

(C) DNA molecule co-localized fluorescence records for experiments with a mixture of labeled Mcm2–7 (Mcm2–7^{JF646}) and Mcm2–7^{25quench}. To investigate whether there were changes in the status of the first Mcm2-Mcm5 gate during loading of the second Mcm2–7 we examined examples where the first bound hexamer was Mcm2–7^{25quench} and the second bound hexamer was Mcm2–7^{JF646}. In both examples shown, Mcm2–7^{25quench} closes before arrival of Mcm2–7^{JF646} (green arrows) and its quenching state did not change when a Mcm2–7^{JF646} binds as the second Mcm2–7 hexamer (red arrows).

(D) Representative DNA molecule co-localized fluorescence records for experiments using labeled Cdc6^{SORT549} and Mcm2–7^{25quench}. In each record, Cdc6 release (red arrows) occurred prior to Mcm2–7 quenching increase (green arrows). The calculated mean dwell time of Cdc6 (12.0 ± 2.2 s [s.e.m.]) is >5-fold shorter than the mean photobleaching lifetime of the Cdc6-bound fluorophore under these conditions (77 ± 18 s [s.e.m.][8]), indicating that most disappearances were due to Cdc6 DNA release, not photobleaching.

(E) Representative DNA molecule co-localized fluorescence records for experiments using labeled ORC^{1SORT549} and Mcm2–7^{25quench}. In each record, ORC release (red arrows) occurred simultaneously with the second Mcm2–7 quenching increase (green arrows). Note: ORC records are vertically offset to facilitate comparison.

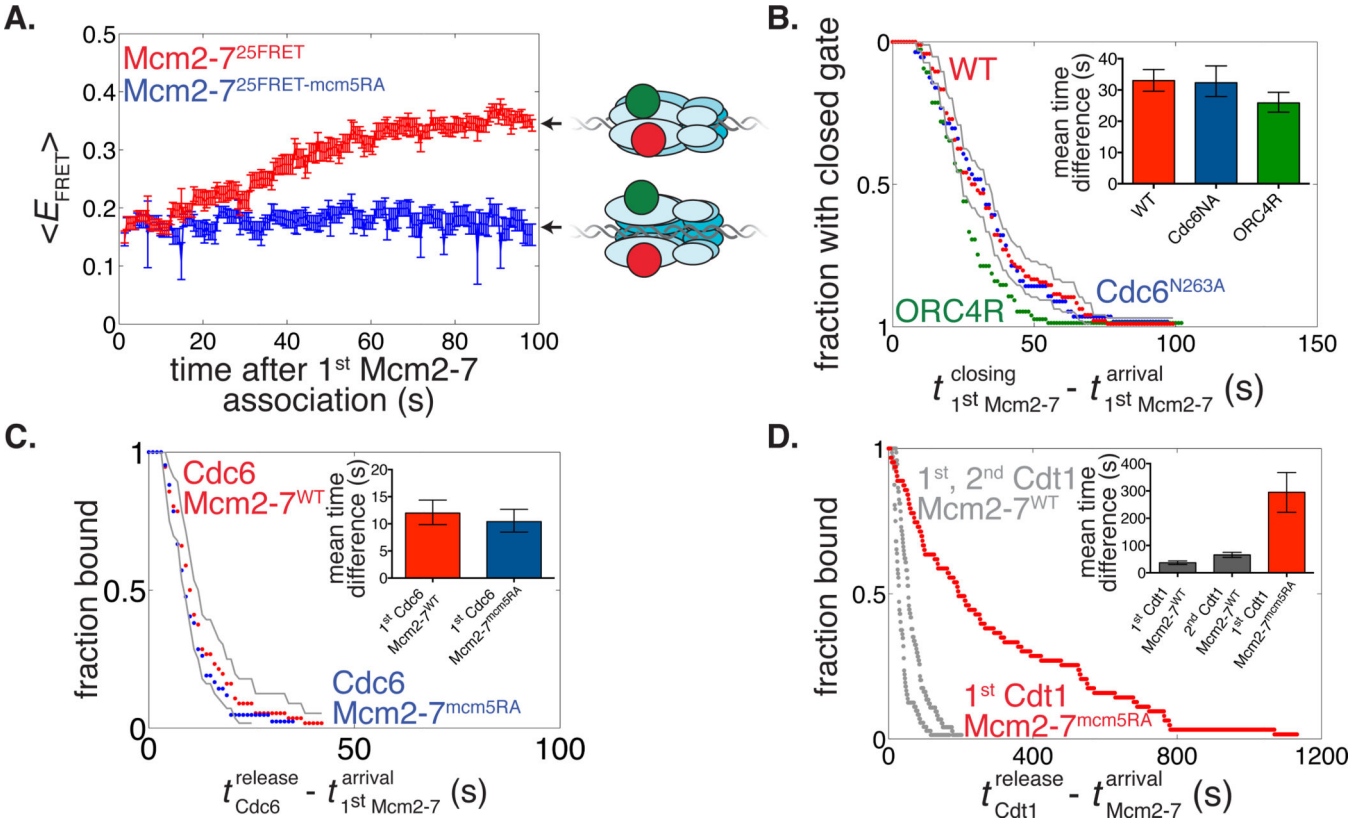

Figure 4. Mcm2–7 ATP hydrolysis is required for gate closing and Cdt1 release

(A) Comparison of population average E_{FRET} values at indicated times after DNA association of first Mcm2–7^{25FRET} (red, N=57 molecules, same data as Supplementary Fig. 2B) or Mcm2–7$^{25FRET\text{-}mcm5RA}$ (blue, N=33 molecules).

(B) Times of gate closing after first Mcm2–7^{25FRET} DNA association for reactions with wild-type ORC–Cdc6 (red, N=96 molecules, 95% C.I. in gray), ORC–Cdc6^{N263A} (blue, N=56 molecules) or ORC4R–Cdc6 (green, N=75 molecules). Inset shows mean gate closure times (± 95% C.I.).

(C) Times of Cdc6^{SORT549} release after association of the first Mcm2–7^{WT} (data from ref [8], red, N=56 molecules, 95% C.I. in gray) or Mcm2–7^{mcm5RA} (blue, N=42 molecules) hexamers. Inset shows mean release times (± 95% C.I.).

(D) Release times (data from ref. 8, gray) of Cdt1^{SORT549} after arrival of the first (N=72) and second (N=74 molecules) Mcm2–7^{WT} compared to release times of Cdt1^{SORT549} after the first Mcm2–7^{mcm5RA} in red (N=63 molecules). Inset shows mean release times ± 95% C.I.s. Mcm2–7^{mcm5RA}-associated Cdt1 release times were underestimated due to remaining associations when imaging was ended (32 of 63 molecules) and Cdt1^{SORT549} photobleaching effects.

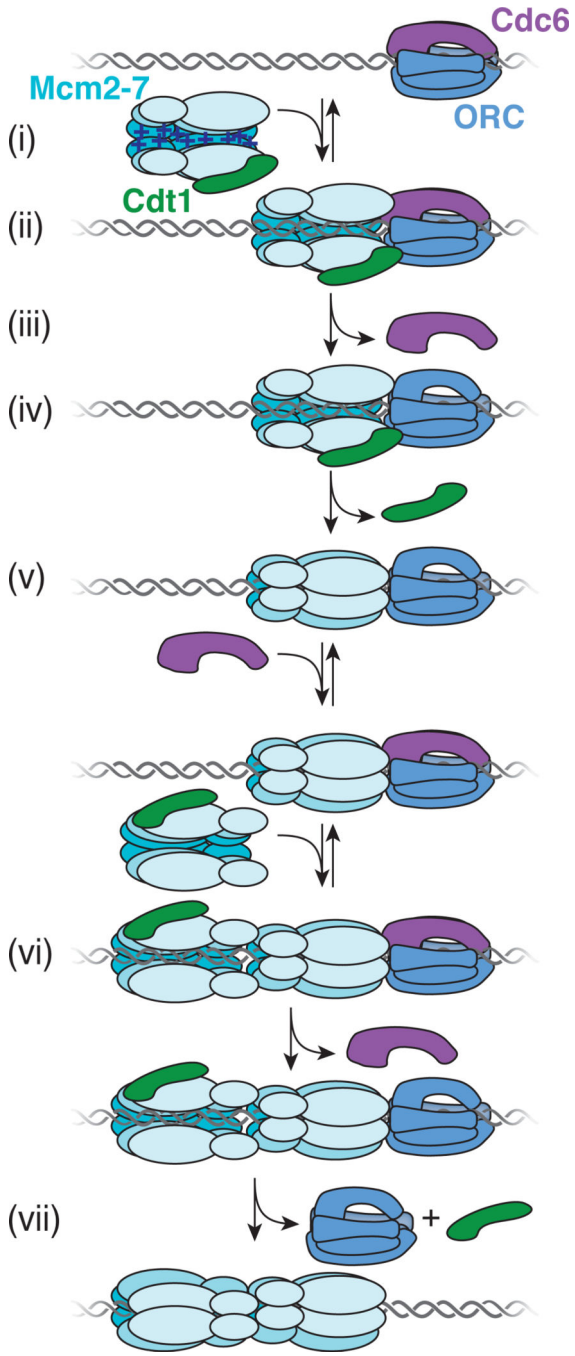

Figure 5. A model for the control of Mcm2–7 gate opening and closing

Prior to DNA binding the Mcm2–7 ring exists predominantly in an open conformation, likely mediated by its positively-charged central channel and bound Cdt1 (i). Association of Mcm2–7 with DNA eliminates charge repulsion, and Cdt1 (together with ORC–Cdc6?) prevents ring closure (ii). The subsequent release of Cdc6 occurs prior to gate closure (iii). Closure of the first Mcm2–7 ring requires ATP hydrolysis by the Mcm5-Mcm3 ATPase (and perhaps other Mcm2–7 ATPases) (iv) and this closure event is associated with Cdt1 release (v). After recruitment of a second Cdc6, a second open Cdt1-Mcm2–7 ring is recruited via

interactions with the first Mcm2–7[8] in a closed state (vi). The subsequent release of the second Cdc6 is followed by the closure of the second Mcm2–7 ring which is simultaneous with the release of Cdt1 and ORC (vii).